The variation of surface propensity of halides with droplet size and temperature

Victor Kwan,[†] Shahrazad M. A. Malek,[‡] and Styliani Consta[*,†]

† *Department of Chemistry, The University of Western Ontario, London, Ontario, Canada N6A 5B7*

‡ *Department of Physics and Physical Oceanography, Memorial University of Newfoundland, Canada, A1B 3X7*

E-mail: sconstas@uwo.ca

Abstract

Relative to a planar interface, nanodroplets are characterized by substantial mass density gradients between the interior and the surface regions and different forces when a sole ion is embedded within them. The radial number density of halide and alkali ions in aqueous clusters with equimolar radius up to $\approx$ 1.4 nm, that corresponds to $\approx$250 H_2O molecules, has been extensively studied. However, the abundance of Cl^-, Br^- and I^- on the surface relative to the bulk interior in these smaller clusters may not be representative of the larger systems. Indeed, here we show that the small droplet sizes with equimolar radius up to $\approx$ 1.4 nm are significantly different in their structure and mass density and thus, in the relative surface abundance of halides from their larger counterparts composed of $\geq$ 800 H_2O molecules (equimolar radius $\geq$ 1.75 nm). Starting from equimolar radius $\approx$ 1.75 nm converging values in the ion location are found. The Cl^- number density profile is the most sensitive to the droplet size and temperature and of the I^- least. The observed trend is that the larger the droplet is, the lower the relative surface abundance of chaotropic halides is. At elevated temperatures Cl^- loses gradually its surface propensity, while I^- still preserves it. The relative interfacial free energy of solvation of the ions is in the range of a few kJ/mol.

Introduction

Aqueous droplets containing alkali and halide ions are omni-present in atmospheric aerosols[1–3] and man-made sprays including ionization methods used in analytical chemistry. An example of the significance of Na^+ and Cl^- ions in aerosols is their effect in the kinetics of photolysis reactions of organic molecules.[4] The fact that the droplet size is a parameter that its variation may lead to systems with different physical and chemical properties has led to studies focusing on different size regimes.

Studies of vapor-water planar interfaces may provide insight into the chemistry in the interface of neutral macroscopic droplets or solid particles.[5–13,13,14,14–30]

On the other end there is also a significant amount of theoretical and experimental research that investigates the local minima in the potential energy surface and free energy of solvation of a single alkali or halogen ion embedded in clusters[31–43,43–48,48–51] The topic is still investigated in order to reconcile differences between computations and experiments and achieve detailed modeling mainly in the smallest clusters via the use of high level quantum chemistry calculations.[52–54]

The location of halide and alkali ions in aqueous clusters, has been considered a resolved matter in the literature. Studies over several decades have reached consensus that the num-

ber density of a single Cl^-, Br^-, I^- is enhanced on the cluster surface, and that F^- and alkali ions lie near the droplet center of mass.[9,32,34,35,39,55,56,56–60] However, the location of the halide ions as a function of droplet size is still unresolved. Stuart and Berne[56] attempted to find the cluster size at which the surface-propensity of a Cl^- ion will decrease and the ion will transfer to the interior. In Ref.[56] the coordination number of Cl^- as a function of cluster size for clusters up to 255 H_2O molecules is estimated and compared with the bulk values. The convergence of the data to the bulk value via extrapolation could not make a prediction perhaps because as we will discuss, in the clusters of this size the single ion number density profile is very different from the larger sizes.

All the computational studies have been performed for clusters composed of a few tens of H_2O molecules, or for clusters with approximately 190 - 255 H_2O molecules using polarizable and non-polarizable models. Specifically, Perera et al.[58] studied clusters with 238 H_2O molecules Stuart and Berne,[56] up to 255 H_2O molecules using OPLS (optimized potential for liquid state) and a charge fluctuating model, Caleman et al.[59] $\approx$ 190 H_2O molecules using a Drude oscillator based polarizable model. To explain the ion location, factors that have been examined are the ion and water polarization, charge and ion size.[55] Stuart and Berne confirmed that Cl^- is located near the surface when a polarizable water model is used and in the cluster interior when a non-polarizable model is used. Wick and Xantheas reported simulations of ions in a slab geometry using a polarizable force field.[57] They considered the factors of size and polarizability for I^- and Cl^-. They found anisotropy in the solvation of the ions. The anisotropy of the solvation structure correlated with polarizability, but it was also found to inversely correlate with anion size.

Our reference point is that a point charge prefers to be in the interior of a droplet because of the two co-operating effects: electrostatic confinement and higher dielectric constant. We have reported that the method of images in electrostatics or the method presented in Ref.,[46] predicts that a single ion in a droplet is always subject to a harmonic potential centered to the droplets' center of mass (COM).

The energy, ΔE_1, related to the distance of the ion from the droplet's COM is given by

$$\Delta E_1(\|\mathbf{r}\|) = K(\varepsilon)\frac{Q^2}{R^3}\|\mathbf{r}\|^2 \qquad (1)$$

where

$$K(\varepsilon) = \frac{\varepsilon - 1}{4\pi\epsilon_0\varepsilon(\varepsilon + 2)} \qquad (2)$$

Q, R and ε are the charge of the ion, the droplet radius and the relative dielectric constant of the solvent, respectively, ϵ_0 is the vacuum permittivity and $\|\mathbf{r}\|^2 = X^2_{\mathrm{COM}} + Y^2_{\mathrm{COM}} + Z^2_{\mathrm{COM}}$ (where $X_{\mathrm{COM}}, Y_{\mathrm{COM}}, Z_{\mathrm{COM}}$ are the coordinates of the droplet's COM). We call this effect "electrostatic confinement" (EC).

Such a force is not present in a planar interface. The EC is more evident for an ion with a charge of at least $\pm 3e$ (where e is the elementary positive charge) found in a droplet with a relatively small radius. For the EC to become evident the radius size will be equal or moderately larger than the radius at the Rayleigh limit.[61–63] The Rayleigh limit is defined as the point where the electrostatic forces balance the surface forces in a droplet. In small droplets the geometric confinement may compete with EC. Moreover, detailed chemical interactions (e.g. charge transfer) may interfere with EC reducing its effect. A simple view of the location of halogen and alkali ions shows consistency with EC. Weakly polarizable ions such as F^-, and the alkali ions are closer to a point charge and they are expected to be found in the interior. The polarizable halides are more complicated because of their large size and polarization. The large size will have a free energy penalty for creating a cavity within the solvent to place the ion. This penalty increases with the ion size.

Even though the smaller clusters have been thoroughly studied,[34,35,39,56,58,59] the abundance of ion on the surface relative to the bulk interior in smaller systems may not be representative of the larger ones. Here we show that the Cl^- and Br^- number density profiles change significantly with the droplet size. The larger the droplet is the surface abundance de-

creases and the interior probability increases. The abundance of the I^- on the surface is not affected as much as that of the other ions by the droplet size. Studies of the location and solvation of ions in mesoscopic clusters (nanodroplets) especially at low temperature or elevated temperature relative to room temperature are still limited.[45,46,58] However, the studies at elevated temperature relative to room temperature are perhaps more relevant nowadays for atmospheric processes since the temperature in Earth is shifted toward higher values. In this study we examined the effect of higher temperature in the number density profiles of halides. We find that among the halides, the Cl^- number density profile is the most vulnerable in increase of temperature. Cl^- probability gradually moves toward the droplet COM and Cl^- loses its surface affinity at temperature 350 K. In the study we assess the outcomes of four force fields, that include polarizable and charge-scaling modeling.

Systems and simulation methods

Molecular dynamics (MD) simulations of charged aqueous droplets containing a sole anion F^-, Cl^-, Br^- and I^- were performed. For comparison, simulations have also been performed with Cs^+. Three non-polarizable parameter sets and one polarizable parameter set were used. The non-polarizable models are: TIP4P/2005 water model[64] with the ion parameters from OPLS-AA,[65] denoted hereafter as OPLS-AA; exactly the same model as before, but the charge of the ions are scaled by a factor of 0.75 suggested by Kirby and Jungwirth,[66] denoted hereafter as OPLS-AA‡; and TIP4P/2005[64] water model with the Madrid-2019-Extended ion parameters (M19),[67,68] where the ions are scaled by a factor of 0.85, denoted hereafter as M19. The polarizable model[69] SWM4-NDP with the CHARMM-Drude force field[70] was used, denoted hereafter as "Drude". The ion parameters are shown in Table S1 in SI. In order to examine the effect of the ion sign in its location in a droplet, simulations with SWM4-NDP and OPLS‡ were performed by changing the sign of the halide ions to positive and keeping all the other parameters the same. The majority of the simulations have been performed for aqueous droplets ranging in size between 200 H_2O molecules ($R_e = 1.1$ nm, where R_e denotes the equimolar radius) to 2000 H_2O molecules ($R_e = 2.5$ nm). Only for Cl^- simulations using SWM4-NDP were performed in a 6000 H_2O droplet ($R_e = 3.7$ nm). The systems and duration of production runs are shown in Table S2 and Table S3 in SI, for the non-polarizable and SWM4-NDP models, respectively. The majority of the simulations have been performed at temperature $T = 300$ K. For comparison simulations have also been performed at $T = 325$ K and $T = 350$ K.

The MD simulations were performed in the canonical ensemble using NAMD version 2.14.[71] The droplet was placed in a spherical cavity of 10 nm radius using the spherical boundary condition as implemented in NAMD in order to maintain a vapor pressure equilibrium. The Newton's equation of motion for each atomic site was integrated using the velocity Verlet algorithm with a time step of 1.0 fs for the polarizable systems and 2.0 fs for the nonpolarizable systems. The trajectories were visualized using VMD 1.9.4a47.[72] All the forces were computed directly without any cutoffs. The temperature was controlled by the Langevin thermostat. For the polarizable systems, NAMD utilizes a dual Langevin thermostat to freeze the Drude oscillators while maintaining the warm degrees of freedom at the desired temperature. The systems were thermalized with the Langevin thermostat at 300 K for the warm degrees of freedom and at 1 K for the Drude oscillators. The damping coefficient for the Langevin thermostat was set to 1/ps.

The mass density and the dielectric constant of the SWM4-NDP water in bulk solution are reported in Ref.[73] Specifically the bulk density of SWM4-NDP at 298.15 K and pressure 1 bar has been reported to be 1.0038 g/cm^3 (experimental: 0.9971 g/cm^3) and dielectric constant 77.8 (experimental: 78.4). At $T = 323$ K and $T = 348$ K (pressure 1 bar) the density has

been reported to be 0.9847 g/cm^3 (experimental: 0.9881 g/cm^3) and 0.9632 g/cm^3 (experimental: 0.9749 g/cm^3, respectively, and the dielectric constant 68.0 (experimental: 70.0) and 58.9 (experimental: 62.4), respectively. It is noted that in the droplet interior the pressure is much higher than 1 bar, thus, the values reported in Ref.[73] for pressure 690 bar are also considered in the data analysis. In the analysis of the H_2O structure, we use the Voronoi volume and the distance of the fifth closest neighbor to the oxygen site of water as described in Ref.[46]

Results and Discussion

Halide surface affinity as a function of droplet size and temperature

Figure 1 (a)-(d) shows the ion number density using the SWM4-NDP model at $T = 300$ K in droplets of various sizes. Table S4 in SI shows the raw data (without division by volume) of residence time (in percentage) of an ion in the droplet's bulk-like interior and exterior. Table 1 shows the data of Table S4 in SI but as concentration and a corresponding equilibrium constant of the exterior over the interior concentration in the droplet. In the next paragraphs the two regions will be defined more precisely.

As it is already known, Cl^-, Br^- and I^- have a surface propensity, while F^- and Cs^+, the largest of the alkali metal ions used here for comparison, are found in the droplet interior.[9,32,34,35,39,56,56–60] However, the relative number density profile of Cl^-, Br^- and I^- changes with the droplet size. The probability to encounter the ion to the bulk-like interior will depend on the volume. To do a democractic comparison, we compare the ratio of the percentage residence time in the exterior among Cl^-, Br^- and I^- within the same droplet size. We find that the Cl^- over I^- ratio decreases from 0.92 in $N = 200$ to 0.72 in $N = 2000$. In order to better understand these differences we examine the H_2O structure in these systems.

Figure 2 provides three diagnostics about the structure of water, the mass density ρ measured in spherical cells around the droplet's center of mass (COM), the denisty ρ_V using the Voronoi volume and d_5 which is the distance of the closest fifth H_2O molecule from the oxygen site of a a H_2O molecule. These diagnostics vary in the same way regardless of the halide ion used. All the diagnostics show that the H_2O density starts to decrease at a distance 0.6 nm from the COM in the droplet with $N = 200$ H_2O molecules ($R_e = 1.1$ nm, where R_e is the equimolar radius), at 1.1 nm in $N = 776$ ($R_e = 1.75$ nm), at 1.8 nm in $N = 2000$ ($R_e = 2.45$ nm), and at 2.9 nm in $N = 6000$ ($R_e = 3.55$ nm).

The estimates of density and pressure in the droplet interior are shown in Table 2. The density in the droplet interior for $N = 200$, is very near the value 1.0286 g/cm^3 reported in Ref.[73] for the bulk SWM4-NDP at 298.15 K at pressure $P = 690$ bar. The interior density of $N = 776$ is also near the value at $P = 690$ bar but slightly lower. It is noted that the Young-Laplace equation predicts a much higher pressure for $N = 200$ and $N = 776$, which raises the question whether SWM4-NDP can adapt its structure in this high pressure. The same question should arise in the simulations presented in Ref.[59] but there is no discussion on this aspect of the problem. As expected, the bulk-like interior density decreases with the increase in the droplet size converging to a bulk value at $T = 298.15$ K and $P = 1.0$ bar when $R_e \approx 1.3$ μm estimated by the Young-Laplace equation.[74] Moreover, the various droplet sizes show differences in the thickness of the exterior region, which includes the subsurface and surface. The difference between the distance at the start of the density decrease and R_e is a constant equal to 0.65 nm, except for $N = 200$ where it is 0.5 nm. The distance of the maximum of the number density of Cl^- from the radius of the bulk-like interior is 2.8 Å in $N = 200$, and converges to the value of 4.5 Å in the larger droplets. Similarly, the distance of the Cl^- and I^- number density maximum increases from 0.4 Å in $N = 200$ to 1.0 Å in the larger droplets. The results show that there is a gradual convergence in the thickness of the external

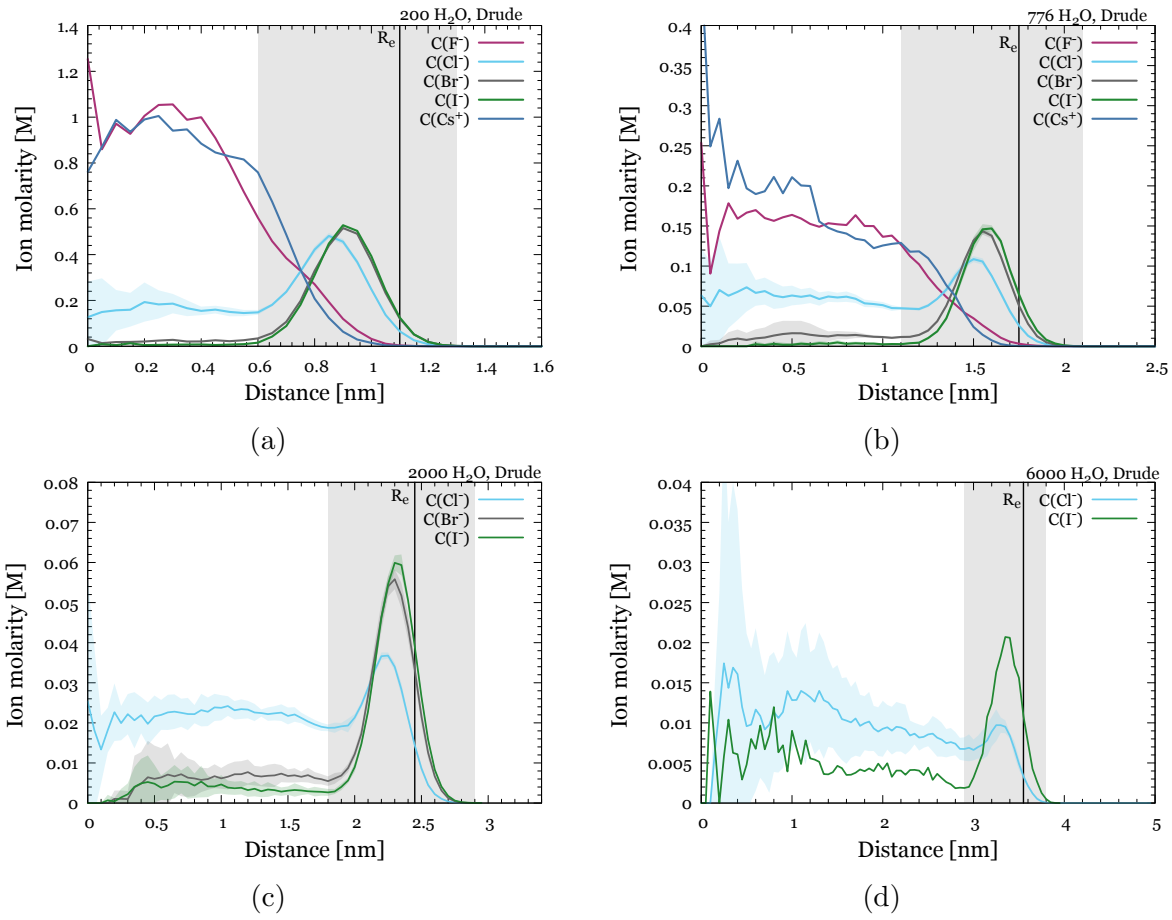

Figure 1: Number density profiles in units of concentration measured from the droplet's center of mass (COM) of an embedded sole ion in an aqueous system comprised (a) $N = 200$, (b) $N = 776$, (c) $N = 2000$, and (d) $N = 6000$. The shaded area indicates the surface region of the droplet. The start point is where the density of H_2O starts to decrease relative to the interior. R_e marks the equimolar radius. Error bars obtained by block averaging over five equally spaced block is shown for Cl^-. The bin size used is 0.5 Å. Simulation length of the systems is shown in Table S3 and they continue to further improve the statistics.

Table 1: Percentage of ion residence time in the droplet's interior and the exterior region (including surface and subsurface) normalized to the volume of the regions. The boundary between the surface and the interior are defined at 6.0 Å, 11.0 Å, 18.0 Å for $N = 200$, 776 and 2000, respectively. The dash lines in the table indicate that simulations have not been performed for these systems because the outcome is expected. Details are in the text.

System	$X^- = F^-$			$X^- = Cl^-$			$X^- = Br^-$			$X^- = I^-$		
	Int.	Ext.	K_{eq}^{F}	Int.	Ext.	K_{eq}^{Cl}	Int.	Ext.	K_{eq}^{Br}	Int.	Ext.	K_{eq}^{I}
$200H_2O$ SWM4-NDP-X^-	82.5	17.5	0.2	32.8	67.2	2.0	6.4	93.6	14.7	2.1	97.9	47.4
$776H_2O$ SWM4-NDP-X^-	80.9	19.1	0.2	49.6	50.4	1.0	15.6	84.4	5.4	4.1	95.9	23.6
$2000H_2O$ SWM4-NDP-X^-	–	–	–	55.9	44.1	0.8	22.4	77.6	3.5	12.5	87.5	7.0
$776H_2O$ OPLS-AA-X^-	83.2	16.8	0.2	78.5	21.5	0.3	76.9	23.1	0.3	63.6	36.4	0.6
$776H_2O$ OPLS-AA‡-X^-	77.3	22.7	0.3	43.4	56.6	1.3	30.0	70.0	2.3	1.9	98.1	50.5
$776H_2O$ M19-X^-	73.7	26.3	0.4	60.1	39.9	0.7	51.5	48.5	0.9	28.8	71.2	2.5

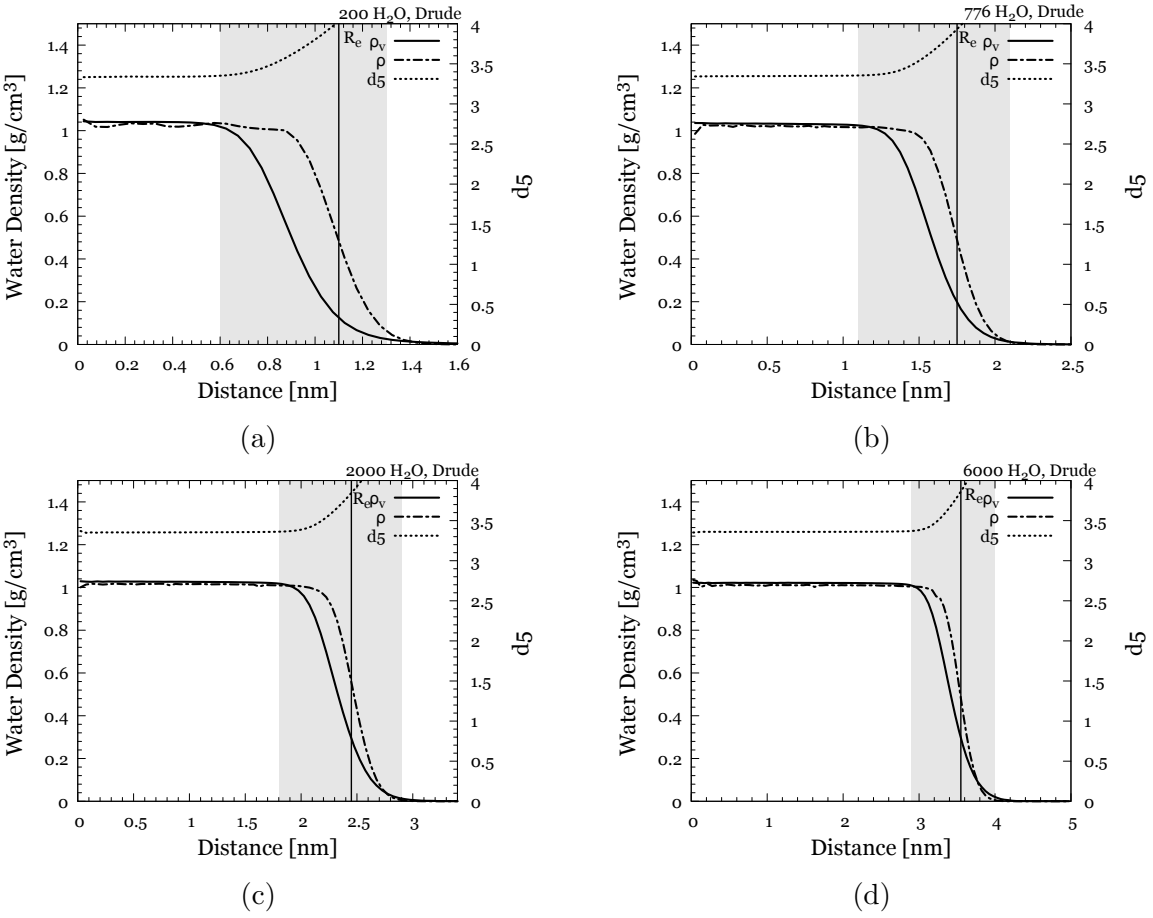

Figure 2: ρ_V, ρ and d_5 of a droplet comprised a sole Cl^- and (a) 200 H_2O, (b) 776 H_2O (c) 2000 H_2O molecules. ρ_V is the density estimated using the Voronoi volume, ρ is the mass density and d_5 (Å) is the distance of the closest fifth H_2O molecule from the oxygen site of a central H_2O molecule. Details are discussed in the text.

region and the location of the maxima of the ion density profiles by increasing the droplet size.

Figure 3 shows that the ions are found in the region where there is charge density variation, which is the same the region where the water density is lower than the bulk-like interior. The grey highlighted region has a thickness of 0.6 nm for the droplet of $N = 200$, and converges to 1.1 nm in the larger droplets.

The combination of Fig. 1, Table S4 in SI and Fig. 2 suggest that as the H_2O density in the bulk-like interior decreases with droplet size, the Cl^-, Br^-, I^- may penetrate easier the H_2O network. This effect becomes more pronounced at $T > 300$ K as shown in Fig. 4. At $T = 350$ K, Cl^- loses its surface propensity. The surface affinity of I^- is least affected by the droplet size and temperature.

In the smallest nanodroplets, even though the interior and exterior regions have the same chemical consistency, they have substantially different organization. For this reason, it may be more suitable to define an equilibrium constant, $K^{\mathrm{X}}_{\mathrm{eq}}$, where X = F, Cl, Br, I, with the sense of a partition coefficient between the two regions. Caleman et al. have used a very similar H_2O model to compute the free energy differences between the ion's state in a droplet composed of approximately 200 H_2O molecules. The interior is defined in the interval (0,7.5 Å) and the surface is defined in the interval (7.5 Å,11 Å), while in our study for approximately the same system size the barrier is found at 6.0 Å. Using the value of 7.5 Å for the barrier location, we estimated a $K^{\mathrm{X}}_{\mathrm{eq}} = 2.02$, 8.9 and 14.4 for Cl^-, Br^-, I^-, respectively, which compares reasonably well with the values 1.6, 7.0 and 13.0 reported in Ref.[59]

Table 2: Estimates of the interior density (ρ_i) for different aqueous droplet sizes (N) and temperature (T) using our simulation data presented in Fig. 2. The pressure (P) was estimated using the Young-Laplace equation. From Ref.[73] the bulk density of SWM4-NDP at 298.15 K and pressure 1 bar has been reported to be 1.0038 g/cm^3 (experimental: 0.9971 g/cm^3). P is estimated using the Young-Laplace equation with surface tension value[69] 67 ± 4 dyn/cm for SMW4-NDP at T = 298.15 K. At T = 325 K and 350 K, P is estimated using the experimental value of surface tension, 67.5 dyn/cm and 64.0 dyn/cm, respectively.

N	T (K)	ρ_i (g/cm^3)	P (bar)
200	300	1.028 ± 0.007	1212 ± 73
776	300	1.021 ± 0.003	766 ± 45
776	325	1.000 ± 0.003	771.4
776	350	0.977 ± 0.004	731.4
2000	300	1.015 ± 0.003	547 ± 33
6000	300	1.015 ± 0.003	378 ± 23

As we showed, in $N = 200$ the partitioning of the ions between the exterior and interior is not representative of the partioning in the larger nanodroplets. Our calculations suggest that droplets with $N \geq 2000$ will be more representative systems to estimate the ion partitioning and the relative interfacial free energy, because SWM4-NDP may not be able to reproduce the appropriate structure in the interior of $N = 200$ and $N = 776$. Simulations at elevated temperature of $T = 325 - 350$ K for $N = 776$ may be also good candidates for performing the simulations using SWM4-NDP. Moreover, for the smallest nanodroplets droplets, the presence of the ion and the much larger relative shape fluctuations, as suggested by Fig. 2 (a) relative to Fig. 2 (b)-(d), will affect the water-water interactions, and thus, one might not be able to infer the dominant interactions that determine the ion location. Estimation of $K_{\rm eq}^{\rm X}$ as a function of temperature will be a more robust approach to extract entropic and enthalpic contributions of the relative interfacial free energy.

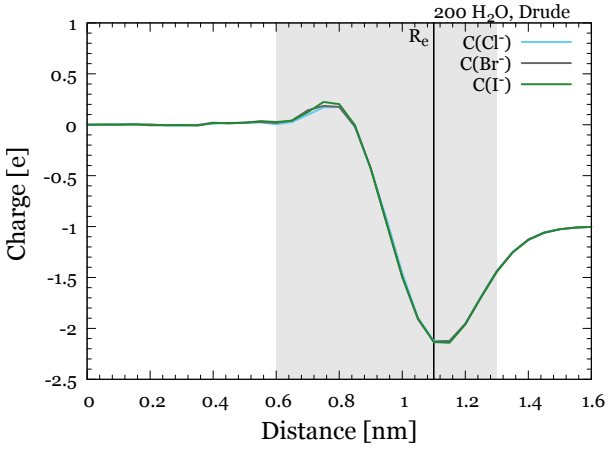

(a)

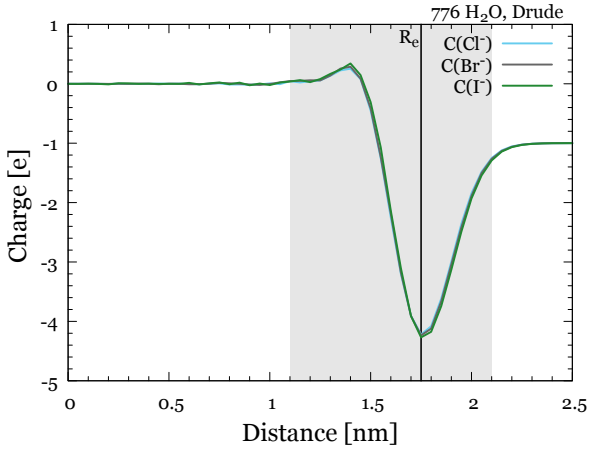

(b)

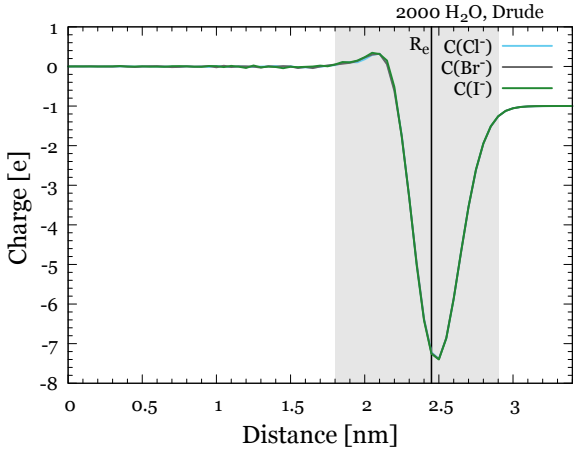

(c)

Figure 3: Cumulative charge distribution function of a droplet comprised a sole ion and (a) $N = 200$, (b) $N = 776$, and (c) $N = 2000$.

The difference in the ΔG between the bulk-like interior and the exterior for certain droplet sizes is reported in Table 3.

The results of the relative free energy can also be useful in studies of droplets with multiple

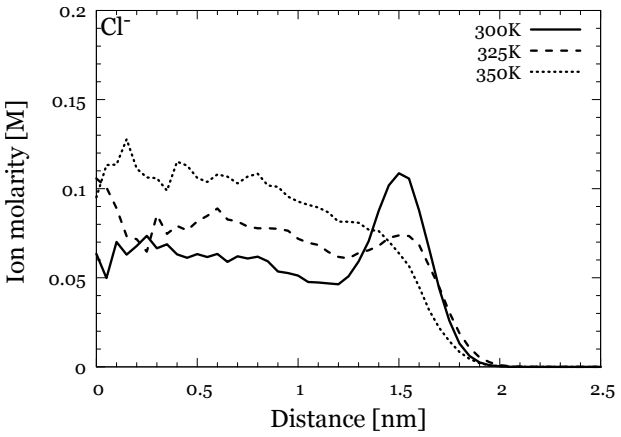

(a)

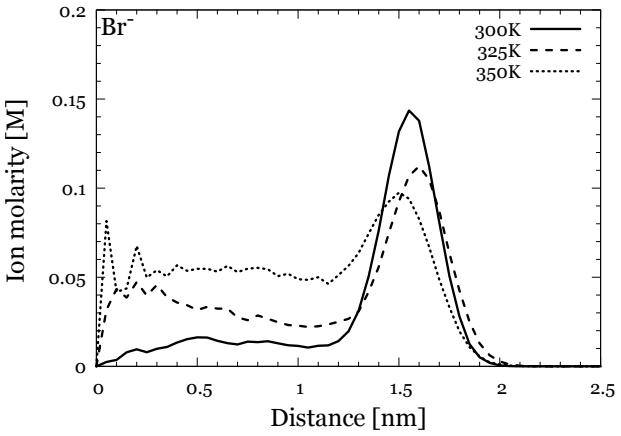

(b)

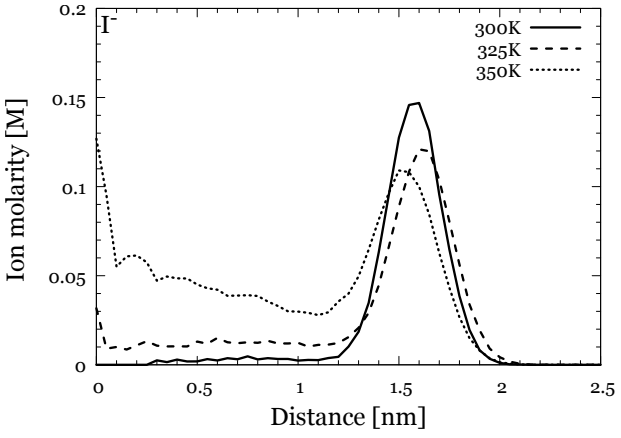

(c)

Figure 4: Number density profile of a droplet comprised 776 H_2O molecules and a sole ion (a) Cl^-, (b) Br^-, (c) I^- at 300K, 325K and 350K.

Table 3: $\Delta\Delta G$ (kJ/mol) for Cl^-, Br^-, and I^- using the K_{eq}^X from Table 1.

N	Cl^-	Br^-	I^-
200	−1.7	−6.7	−9.6
776	0.0	−4.2	−7.9
2000	0.6	−3.1	−4.8

ions of the same sign. If we estimate the single ion relative interfacial free energy, we deduce that we can use this quantity in the ion evaporation model[75] for computing the relative rate of ion ejection from droplets with multiple Cl^-, Br^- and I^- ions. Our previous research[76] has shown that multiple Cl^-, I^- (expected also for Br^-) ions in the outer layers of SWM4-NDP droplets are found at the same distance from the droplet surface as the single ion. Thus, for droplets larger than 1000 H_2O molecules, where the ion motions are uncorrelated, the sole halide interfacial solvation energy may be used to compute the rate of single ion evaporation.

Factors that affect the halide ion surface affinity

Scaled charge force fields We examined the effect of the force field in predicting the sole halide surface affinity. Specifically, we tested the TIP4P/2005 water model, and the newer models with scaled charge OPLS-AA‡, and M19. Details are described in the section "Systems and simulation methods". The comparison of the ion number density profiles are shown in Fig. S1 in SI and the raw date of the ion residence time Table S4 in SI. Figure S2 in SI shows the ion-oxygen site radial distribution functions (RDFs) for the tested models. If one takes the SMW4-NDP as the baseline, the OPLS-AA‡ model best approximates the polarizable model. The M19 model intends to reproduce the structure of aqueous solutions and results in a concentration profile that resembles that of multiple ions in solution. The unscaled OPLS-AA model and other non-polarizable models do not introduce any surface preference as it has already been discussed in the literature.[56] The charge scaling method

originates from the need to approximate the electrostatic screening that arises from the electronic polarization in bulk water without resorting to explicit polarization. Therefore, the charge scaled force field yields a weaker than expected interaction between the ion and water in the surface and subsurface. In the OPLS-AA‡ case, this result in an ion number density profile near the surface having only qualitative agreement with the SWM4-NDP model.

It is interesting to compare the RDFs of TIP4P/2005 and SWM4-NDP models in bulk solution at $T = 273.15$ K and at elevated pressure. The comparison of the RDF reported in Refs.[64,73] at $T = 273.15$ K and $P = 1$ bar shows that TIP4P/2005 is more structured than SWM4-NDP. It has been reported in Ref.[73] that the O-H and O-O SWM4-NDP RDFs and diffusion coefficients of bulk solution at $T = 273.15$ K pressure up to 690 bar do not change, however, we observe in Fig. 4 of Ref.[73] a small loss of structure in the second coordination shell of O-O at $P = 690$ bar.

Ion charge and polarization We simulate a droplet containing a sole Cl^+, Br^+ and I^+ with OPLS-AA‡ in order to examine the role of the sign of the charge. The number density profiles are shown in Fig. S3 in SI. The results from the polarizable model shows that X^+ does not have a preference toward the surface at the size of $200H_2O$, which is consistent with the result of Caleman et al. in Ref.[59]) and $776H_2O$. However, the OPLS-AA† shows that the positively charged analogue of halides are also attached to the surface. It appears that in OPLS‡ the correction made to reproduce the negative ions, also differentiates the positive ions. The correction is in the charge, so the charge density change. We accept as true that the positive ions are not differentiated and are found near the center. This shows that the charge density alone may be the factor that differentiates the negative ions and positive ions in this model. Simulations were also performed for a sole Cl^- in $N = 200$ using the SWM4-NDP model by eliminating the Cl^- polarization and keeping all the other parameters the same. We found that Cl^- loses its surface affinity and resides in the interior. All the tests suggest that by changing one of the parameters in a model we cannot deduce the factors that determine the ion location because all the parameters are related in order to reproduce certain properties. Thus, changing the ion parameters to determine the dominant effect is not a fruitful path within the force field framework.

Conclusion

1. We showed that the small droplet sizes with equimolar radius up to $\approx 1.1 - 1.4$ nm are significantly different in their structure and mass density and thus, in the relative surface abundance of halides from their larger counterparts composed of ≥ 800 H_2O molecules (equimolar radius ≥ 1.75 nm). From equimolar radius ≈ 1.75 nm we start seeing converging values in the ion location. Cl^- number density is the most sensitive to the droplet size and temperature while I^- is least sensitive. The trend that we identify is that the larger the droplet is, the lower the relative surface abundance of chaotropic halides is. At elevated temperatures Cl^- loses gradually its surface propensity, while I^- still preserves it.

2. We estimated the relative interfacial free energy of solvation of the ions, which is in the range of a few kJ/mol.

3. The interplay of factors that lead to the chaotropic halides propensity on an aqueous planar interface may not be the same as in a droplet because of the large mass density gradients in the droplet and the existence of forces such as the electrostatic confinement, which does not exist in the planar interface.

4. We assessed the quality of the scaled models optimized for the bulk solution in predicting the location of the ions. The OPLS‡ appears to be the closest to the the SWM4-NDP in simulations of droplets with ions. This may be important in

the atomistic modeling not only of a sole ion in a droplet, but also of multiple excess ions in a droplet. The use of OPLS‡ may extend the system sizes accessible to atomistic modeling relative to a polarizable model that is more computationally expensive. The use of OPLS‡ may assist to explore the ion evaporation mechanism for negative ions in droplets that contain tens of thousands of H_2O molecules, where it is expected to show release of simple ions.

Supporting Information

(S1.) System and simulation parameters; (S2.) Number density of the sole ion in an aqueous droplet using various force fields; (S3.) Comparison of the radial distribution functions (RDFs) of Ion-Oxygen for the various models; (S4.) Potentials of mean force (PMFs) for the ions along the distance from the droplet's COM reaction coordinate; (S5.) Number density profiles for X^+ in aqueous droplets using different force fields.

Acknowledgments

S.C. thanks Prof. D. Frenkel, Yusuf Hamied Department of Chemistry, University of Cambridge, UK, Prof. R. Kapral, Department of Chemistry, University of Toronto, Prof. B. J. Finlayson-Pitts and Prof. J. Smith as well as the group members, Dr. Lisa M. Wingen, Dr. Veronique Perraud, and Dr. Yiming Qin, Department of Chemistry, University of California, Irvine, Prof. S. S. Xantheas, Pacific Northwest National Laboratory, Prof. Ivan Saika-Voivod, Department of Physics and Physical Oceanography, Memorial University of Newfoundland, and Dr. Anatoly Malevanets for insightful discussions on ion-cluster interactions. S.C. acknowledges an NSERC-Discovery grant (Canada) for funding this research. V.K. acknowledges the Province of Ontario and the University of Western Ontario for the Queen Elizabeth II Graduate Scholarship in Science and Technology. Digital Research Alliance of Canada is acknowledged for providing the computing facilities.

References

(1) Vaida, V. Perspective: Water cluster mediated atmospheric chemistry. *J. Chem. Phys.* **2011**, *135*, 020901.

(2) Knipping, E.; Lakin, M.; Foster, K.; Jungwirth, P.; Tobias, D.; Gerber, R.; Dabdub, D.; Finlayson-Pitts, B. Experiments and simulations of ion-enhanced interfacial chemistry on aqueous NaCl aerosols. *Science* **2000**, *288*, 301–306.

(3) Gerber, R. B.; Varner, M. E.; Hammerich, A. D.; Riikonen, S.; Murdachaew, G.; Shemesh, D.; Finlayson-Pitts, B. J. Computational studies of atmospherically-relevant chemical reactions in water clusters and on liquid water and ice surfaces. *Acc. Chem. Res.* **2015**, *48*, 399–406.

(4) Kahan, T.; Kwamena, N.-O.; Donaldson, D. Different photolysis kinetics at the surface of frozen freshwater vs. frozen salt solutions. *Atmospheric Chem. Phys.* **2010**, *10*, 10917–10922.

(5) Enami, S.; Colussi, A. J. Long-range specific ion-ion interactions in hydrogen-bonded liquid films. *J. Chem. Phys.* **2013**, *138*, 184706.

(6) Enami, S.; Colussi, A. J. Ion-Specific Long-Range Correlations on Interfacial Water Driven by Hydrogen Bond Fluctuations. *J. Phys. Chem. B* **2014**, *118*, 1861–1866.

(7) Jungwirth, P.; Tobias, D. J. Surface effects on aqueous ionic solvation: A molecular dynamics simulation study of NaCl at the air/water interface from infinite dilution to saturation. *J. Phys. Chem. B* **2000**, *104*, 7702–7706.

(8) Otten, D. E.; Shaffer, P. R.; Geissler, P. L.; Saykally, R. J. Elucidating the mechanism

of selective ion adsorption to the liquid water surface. *Proc. Natl. Acad. Sci. U.S.A.* **2012**, *109*, 701–705.

(9) Petersen, P. B.; Saykally, R. J. On the nature of ions at the liquid water surface. *Annu. Rev. Phys. Chem.* **2006**, *57*, 333–364.

(10) Onorato, R. M.; Otten, D. E.; Saykally, R. J. Measurement of bromide ion affinities for the air/water and dodecanol/water interfaces at molar concentrations by UV second harmonic generation spectroscopy. *J. Phys. Chem. C* **2010**, *114*, 13746–13751.

(11) Smith, J. W.; Saykally, R. J. Soft x-ray absorption spectroscopy of liquids and solutions. *Chem. Rev.* **2017**, *117*, 13909–13934.

(12) Baer, M. D.; Mundy, C. J. Toward an understanding of the specific ion effect using density functional theory. *J. Phys. Chem. Lett.* **2011**, *2*, 1088–1093.

(13) Adel, T.; Ng, K. C.; Vazquez de Vasquez, M. G.; Velez-Alvarez, J.; Allen, H. C. Insight into the Ionizing Surface Potential Method and Aqueous Sodium Halide Surfaces. *Langmuir* **2021**, *37*, 7863–7874.

(14) Beck, T. L. The influence of water interfacial potentials on ion hydration in bulk water and near interfaces. *Chem. Phys. Lett.* **2013**, *561*, 1–13.

(15) Tobias, D. J.; Hemminger, J. C. Getting specific about specific ion effects. *Science* **2008**, *319*, 1197–1198.

(16) Tielrooij, K.; Garcia-Araez, N.; Bonn, M.; Bakker, H. Cooperativity in ion hydration. *Science* **2010**, *328*, 1006–1009.

(17) Vrbka, L.; Mucha, M.; Minofar, B.; Jungwirth, P.; Brown, E. C.; Tobias, D. J. Propensity of soft ions for the air/water interface. *Current opinion in colloid & interface science* **2004**, *9*, 67–73.

(18) Bastos-González, D.; Pérez-Fuentes, L.; Drummond, C.; Faraudo, J. Ions at interfaces: the central role of hydration and hydrophobicity. *Current opinion in colloid & interface science* **2016**, *23*, 19–28.

(19) Levin, Y. Polarizable ions at interfaces. *Phys. Rev. Lett.* **2009**, *102*, 147803.

(20) Chang, T.-M.; Dang, L. X. Recent advances in molecular simulations of ion solvation at liquid interfaces. *Chem. Rev.* **2006**, *106*, 1305–1322.

(21) Benjamin, I. Theoretical study of ion solvation at the water liquid–vapor interface. *J. Chem. Phys.* **1991**, *95*, 3698–3709.

(22) Onuki, A. Ginzburg-Landau theory of solvation in polar fluids: Ion distribution around an interface. *Phys. Rev. E* **2006**, *73*, 021506.

(23) Chakraborty, D.; Patey, G. How crystals nucleate and grow in aqueous NaCl solution. *J. Phys. Chem. Lett.* **2013**, *4*, 573–578.

(24) Ou, S.-C.; Cui, D.; Patel, S. Molecular modeling of ions at interfaces: Exploring similarities to hydrophobic solvation through the lens of induced aqueous interfacial fluctuations. *Phys. Chem. Chem. Phys.* **2016**, *18*, 30357–30365.

(25) Dang, L. X. Computational study of ion binding to the liquid interface of water. *J. Phys. Chem. B* **2002**, *106*, 10388–10394.

(26) Duignan, T. T.; Zhao, X. S. The Born model can accurately describe electrostatic ion solvation. *Physical Chemistry Chemical Physics* **2020**, *22*, 25126–25135.

(27) Noah-Vanhoucke, J.; Geissler, P. L. On the fluctuations that drive small ions toward, and away from, interfaces between polar liquids and their vapors. *Proc. Natl. Acad. Sci. U.S.A.* **2009**, *106*, 15125–15130.

(28) Jubb, A. M.; Hua, W.; Allen, H. C. Environmental chemistry at vapor/water interfaces: insights from vibrational sum frequency generation spectroscopy. *Annu. Rev. Phys. Chem.* **2012**, *63*, 107–130.

(29) Castro, A.; Bhattacharyya, K.; Eisenthal, K. B. Energetics of adsorption of neutral and charged molecules at the air/water interface by second harmonic generation: Hydrophobic and solvation effects. *J. Chem. Phys.* **1991**, *95*, 1310–1315.

(30) Ren, Y.; Soni, A.; Kumar, A.; Bertram, A. K.; Patey, G. Effects of pH on Ice Nucleation by the α-Alumina (0001) Surface. *The Journal of Physical Chemistry C* **2022**, *126*, 19934–19946.

(31) Briant, C.; Burton, J. Molecular dynamics study of the structure and thermodynamic properties of argon microclusters. *J. Chem. Phys.* **1975**, *63*, 2045–2058.

(32) Wilson, M. A.; Pohorille, A. Interaction of monovalent ions with the water liquid–vapor interface: A molecular dynamics study. *J. Chem. Phys.* **1991**, *95*, 6005–6013.

(33) Lu, D.; Singer, S. J. Ion solvation in model polar clusters. *The Journal of chemical physics* **1996**, *105*, 3700–3714.

(34) Perera, L.; Berkowitz, M. L. Many-body effects in molecular dynamics simulations of Na+ (H2O) n and Cl-(H2O) n clusters. *J. Chem. Phys.* **1991**, *95*, 1954–1963.

(35) Perera, L.; Berkowitz, M. L. Erratum: Many-body effects in molecular dynamics simulations of Na+ (H2O) n and Cl-(H2O) n clusters [J. Chem. Phys. 95, 1954 (1991)]. *J. Chem. Phys.* **1993**, *99*, 4236–4237.

(36) Fifen, J. J.; Agmon, N. Structure and spectroscopy of hydrated sodium ions at different temperatures and the cluster stability rules. *J. Chem. Theory Comput.* **2016**, *12*, 1656–1673.

(37) Kelly, C. P.; Cramer, C. J.; Truhlar, D. G. Aqueous solvation free energies of ions and ion- water clusters based on an accurate value for the absolute aqueous solvation free energy of the proton. *J. Phys. Chem. B* **2006**, *110*, 16066–16081.

(38) Gorlova, O.; DePalma, J. W.; Wolke, C. T.; Brathwaite, A.; Odbadrakh, T. T.; Jordan, K. D.; McCoy, A. B.; Johnson, M. A. Characterization of the primary hydration shell of the hydroxide ion with H2 tagging vibrational spectroscopy of the OH^--(H2O) n= 2, 3 and OD^--(D2O) n= 2, 3 clusters. *J. Chem. Phys.* **2016**, *145*, 134304.

(39) Perera, L.; Berkowitz, M. L. Stabilization energies of Cl-, Br-, and I- ions in water clusters. *The Journal of chemical physics* **1993**, *99*, 4222–4224.

(40) Perera, L.; Berkowitz, M. L. Structure and dynamics of Cl-(H2O) 20 clusters: The effect of the polarizability and the charge of the ion. *J. Chem. Phys.* **1992**, *96*, 8288–8294.

(41) Lynden-Bell, R.; Rasaiah, J.; Noworyta, J. Using simulation to study solvation in water. *Pure Appl. Chem.* **2001**, *73*, 1721–1731.

(42) Bagchi, B.; Jana, B. Solvation dynamics in dipolar liquids. *Chem. Soc. Rev.* **2010**, *39*, 1936–1954.

(43) Miller, D. J.; Lisy, J. M. Hydrated Alkali-Metal Cations: Infrared Spectroscopy and ab Initio Calculations of M+ (H2O) x= 2-5Ar cluster ions for M= Li, Na, K, and Cs. *J. Am. Chem. Soc.* **2008**, *130*, 15381–15392.

(44) Thaunay, F.; Ohanessian, G.; Clavaguera, C. Dynamics of ions in a water drop using the AMOEBA polarizable force field. *Chem. Phys. Lett.* **2017**, *671*, 131–137.

(45) Burnham, C. J.; Petersen, M. K.; Day, T. J.; Iyengar, S. S.; Voth, G. A.

The properties of ion-water clusters. II. Solvation structures of Na+, Cl-, and H+ clusters as a function of temperature. *J. Chem. Phys.* **2006**, *124*, 024327.

(46) Malek, S. M. A.; Kwan, V.; Saika-Voivod, I.; Consta, S. Low Density Interior in Supercooled Aqueous Nanodroplets Expels Ions to the Subsurface. *J. Am. Chem. Soc.* **2021**, *143*, 13113–13123.

(47) Sharma, B.; Chandra, A. Born–Oppenheimer Molecular Dynamics Simulations of a Bromate Ion in Water Reveal Its Dual Kosmotropic and Chaotropic Behavior. *The Journal of Physical Chemistry B* **2018**, *122*, 2090–2101.

(48) Chakrabarty, S.; Williams, E. R. The effect of halide and iodate anions on the hydrogen-bonding network of water in aqueous nanodrops. *Phys. Chem. Chem. Phys.* **2016**, *18*, 25483–25490.

(49) Stachl, C. N.; Williams, E. R. Effects of temperature on Cs+ (H2O) 20 clathrate structure. *J. Phys. Chem. Lett.* **2020**, *11*, 6127–6132.

(50) Muralidharan, A.; Pratt, L.; Chaudhari, M.; Rempe, S. Quasi-chemical theory for anion hydration and specific ion effects: Cl-(aq) vs. F-(aq). *Chem. Phys. Lett.: X* **2019**, *4*, 100037.

(51) Cabarcos, O. M.; Weinheimer, C. J.; Martinez, T. J.; Lisy, J. M. The solvation of chloride by methanol—surface versus interior cluster ion states. *The Journal of chemical physics* **1999**, *110*, 9516–9526.

(52) Galib, M.; Baer, M.; Skinner, L.; Mundy, C.; Huthwelker, T.; Schenter, G.; Benmore, C.; Govind, N.; Fulton, J. L. Revisiting the hydration structure of aqueous Na+. *J. Chem. Phys.* **2017**, *146*, 084504.

(53) Wang, P.; Shi, R.; Su, Y.; Tang, L.; Huang, X.; Zhao, J. Hydrated sodium ion clusters [Na+ (H2O) n (n= 1–6)]: an ab initio study on structures and noncovalent interaction. *Frontiers in chemistry* **2019**, *7*, 624.

(54) Heindel, J. P.; Xantheas, S. S. The many-body expansion for aqueous systems revisited: II. Alkali metal and halide ion–water interactions. *Journal of Chemical Theory and Computation* **2021**, *17*, 2200–2216.

(55) Wise, P. K.; Slipchenko, L. V.; Ben-Amotz, D. Ion-Size Dependent Adsorption Crossover on the Surface of a Water Droplet. *J. Phys. Chem. B* **2023**,

(56) Stuart, S. J.; Berne, B. Effects of polarizability on the hydration of the chloride ion. *J. Phys. Chem.* **1996**, *100*, 11934–11943.

(57) Wick, C. D.; Xantheas, S. S. Computational investigation of the first solvation shell structure of interfacial and bulk aqueous chloride and iodide ions. *J. Phys. Chem. B* **2009**, *113*, 4141–4146.

(58) Herce, D. H.; Perera, L.; Darden, T. A.; Sagui, C. Surface solvation for an ion in a water cluster. *J. Chem. Phys.* **2005**, *122*, 024513.

(59) Caleman, C.; Hub, J. S.; van Maaren, P. J.; van der Spoel, D. Atomistic simulation of ion solvation in water explains surface preference of halides. *Proc. Natl. Acad. Sci. U.S.A.* **2011**, *108*, 6838–6842.

(60) Jungwirth, P.; Tobias, D. J. Specific ion effects at the air/water interface. *Chem. Rev.* **2006**, *106*, 1259–1281.

(61) Rayleigh, L. XX. On the equilibrium of liquid conducting masses charged with electricity. *Philos. Mag.* **1882**, *14*, 184–186.

(62) Hendricks, C.; Schneider, J. Stability of a conducting droplet under the influence of surface tension and electrostatic forces. *Am. J. Phys.* **1963**, *31*, 450–453.

(63) Consta, S.; Malevanets, A. Disintegration mechanisms of charged nanodroplets: novel systems for applying methods of activated processes. *Mol. Simul.* **2015**, *41*, 73–85.

(64) Abascal, J. L. F.; Vega, C. A general purpose model for the condensed phases of water: TIP4P/2005. *J. Phys. Chem* **2005**, *123*, 234505.

(65) Aqvist, J. Ion-water interaction potentials derived from free energy perturbation simulations. *J. Phys. Chem.* **1990**, *94*, 8021–8024.

(66) Kirby, B. J.; Jungwirth, P. Charge scaling manifesto: A way of reconciling the inherently macroscopic and microscopic natures of molecular simulations. *J. Phys. Chem. Lett.* **2019**, *10*, 7531–7536.

(67) Zeron, I.; Abascal, J.; Vega, C. A force field of Li+, Na+, K+, Mg2+, Ca2+, Cl-, and SO 4 2- in aqueous solution based on the TIP4P/2005 water model and scaled charges for the ions. *J. Chem. Phys.* **2019**, *151*, 134504.

(68) Blazquez, S.; Conde, M.; Abascal, J.; Vega, C. The Madrid-2019 force field for electrolytes in water using TIP4P/2005 and scaled charges: Extension to the ions F-, Br-, I-, Rb+, and Cs+. *J. Chem. Phys.* **2022**, *156*, 044505.

(69) Lamoureux, G.; Harder, E.; Vorobyov, I. V.; Roux, B.; MacKerell, A. D. A polarizable model of water for molecular dynamics simulations of biomolecules. *Chem. Phys. Lett.* **2006**, *418*, 245–249.

(70) Jiang, W.; Hardy, D. J.; Phillips, J. C.; MacKerell, A. D.; Schulten, K.; Roux, B. High-Performance Scalable Molecular Dynamics Simulations of a Polarizable Force Field Based on Classical Drude Oscillators in NAMD. *J. Phys. Chem. Lett.* **2011**, *2*, 87–92, PMID: 21572567.

(71) Phillips, J. C.; Braun, R.; Wang, W.; Gumbart, J.; Tajkhorshid, E.; Villa, E.; Chipot, C.; Skeel, R. D.; Kalé, L.; Schulten, K. Scalable molecular dynamics with NAMD. *J. Comput. Chem.* **2005**, *26*, 1781–1802.

(72) Humphrey, W.; Dalke, A.; Schulten, K. VMD: Visual Molecular Dynamics. *J. Mol. Graphics* **1996**, *14*, 33–38.

(73) Stukan, M. R.; Asmadi, A.; Abdallah, W. Bulk properties of SWM4-NDP water model at elevated temperature and pressure. *Journal of Molecular Liquids* **2013**, *180*, 65–69.

(74) Behroozi, F. A Fresh Look at the Young-Laplace Equation and Its Many Applications in Hydrostatics. *The Physics Teacher* **2022**, *60*, 358–361.

(75) Iribarne, J. V.; Thomson, B. A. On the evaporation of small ions from charged droplets. *J. Chem. Phys.* **1976**, *64*, 2287–2294.

(76) Kwan, V.; Consta, S. Conical Shape Fluctuations Determine the Rate of Ion Evaporation and the Emitted Cluster Size Distribution from Multicharged Droplets. *J. Phys. Chem. A* **2022**, *126*, 3229–3238.